

Real-time automatic identification ear diseases using a deep learning model

Xinyu Zeng

People's Hospital of Shenzhen Baoan District

Zifan Jiang

Hebei University of Technology

Wen Luo

Guangdong Polytechnic Normal University

Honggui Li

First Affiliated Hospital of Guangzhou University of Chinese Medicine

Hongye Li

Zhuhai Vocational School of Polytechnic

Guo Li

Cloud & Gene AI Research Institute

Jingyong Shi

People's Hospital of Shenzhen Baoan District

Kangjie Wu

People's Hospital of Shenzhen Baoan District

Tong Liu

People's Hospital of Shenzhen Baoan District

Xing Lin

People's Hospital of Shenzhen Baoan District

Fusen Wang

People's Hospital of Shenzhen Baoan District

Zhenzhang Li (✉ zhenzhangli@gpnu.edu.cn)

Guangdong Polytechnic Normal University

Research Article

Keywords: deep learning model, ear diseases

Posted Date: February 15th, 2021

DOI: <https://doi.org/10.21203/rs.3.rs-156314/v1>

Abstract

Early detection and appropriate medical treatment is of great use for ear disease. However, a new diagnostic strategy is necessary in the absence of experts and relatively low diagnostic accuracy, in which deep learning plays an important role. This paper puts forward a mechanic learning model which uses abundant otoscope image data gained in the clinical cases in order to achieve automatic diagnosis of ear diseases in real time. A total of 20,542 endoscopic images were employed to train nine common deep convolution neural networks. According to the characteristics of eardrum and external auditory canal, eight kinds of ear diseases were classified, involving the majority of ear diseases, such as normal, Cholesteatoma of middle ear, Chronic suppurative otitis media, External auditory cana bleeding, Impacted cerumen, Otomycosis external, Secretory otitis media, Tympanic membrane calcification. After we evaluate these optimization schemes, two best performance models are selected to combine the ensemble classifiers with real-time automatic classification. Based on accuracy and training time, we choose a transferring learning model based on DensNet-BC169 and DensNet-BC1615, getting a result that each model has obvious improvement by using these two ensemble classifiers, and has average accuracy of 95.59%. Considering the dependence of classifier performance on data size in transfer learning, we evaluate the high accuracy of the current model that can be attributed to large databases. Current studies are unparalleled regarding disease diversity and diagnostic precision. The real-time classifier trains the data under different acquisition conditions, which is suitable for the real cases. According to this study, in the clinical case, deep learning model is of great use in early detection and remedy of ear diseases.

Introduction

As is known to us all, the sense of hearing is considered as one of the most important five senses, since the sense of hearing is human lives mainly rely on [1]. However, as a common disease, if not be received early and treated validly, ear disease may leave some negative effecton, for example hearing impairment. In the estimation of ear diseases in the clinic, conventional otoscopy or otoendoscopy is an important component of physical examination at the first step. However, otoscopy or otoendoscopy used in diagnosis can be easily misdiagnosed for non-otolaryngologists [2]. A research of Pichichero, Poole [3], for example, found that the average accuracy of otitis media diagnosed by 514 pediatricians was only 50%. Such low diagnostic accuracy hinted that, without the assistance of supplementary resources, testing the diagnosis of ear disease will be difficult, even for experts. Based on such a situation, there is a great need to find a new diagnostic strategy to improve diagnostic accuracy.

In these years, deep learning has acted as a promising method for image recognition or classification, is the foundation of automatic image perceiving, processing and deciding, and has been a heated topic in the area of computer vision for a long time [4, 5]. Deep learning has been applied in several medical imaging areas, such as development and validation of a deep learning algorithm for detection of diabetic retinopathy in retinal fundus photographs [6], large-scale deep learning for computer aided detection of mammographic lesions [7]. In these deep learning applications, deep convolutional neural networks

(CNNs) [8] is playing a very important role in image recognition or classification. Very little prior professional knowledge is needed to input during the training procedure of deep CNNs models. Emerged as a feature extractor, some pretrained deep CNNs can rival or excel the execution of domain-specific, handcrafted features [9–12].

To the best of our knowledge, the purpose of this research is to set up an automatic discriminating system for ear diseases by a deep learning model. The performance of twelve public models were evaluated by accuracy and training-validation time. Based on the assessment results, two best models among 12 models were chosen to build an ensemble classifier which then can design and accomplish a real-time automatic identification ear diseases system.

Materials And Methods

Patient selection and data preprocessing

In this study, our dataset was obtained from 41,056 patients who were diagnosed in the department of otolaryngology in the people's hospital of Shenzhen Baoan district, from July 2016 to August 2019. Usually, patients got their eardrums and external auditory canal (EAC) photos via a conchoscope upon visit. These images were got by using standard endoscopes (Matrix E2, XION GmbH, Berlin, Germany) tethered to Olympus CV-170 digital endovision camera systems (Olympus Corporation, Tokyo, Japan). The resolution rate of these images is 586×583 pixels. In order to unify graph data and keep the original shape, we uniformly cropped and scaled these images with a size of 448×448 pixels with a ratio of 1:1. We chose 20,542 images, about 53.55% of the total candidate images. Male 11,797. female 8,745. occupied 57.43% and 42.57% of the total number of the selected images, respectively, as shown in **Table 1**. According to the age, aged (0,10] years have the maximum (22.187%) , aged (30,40] years (21.169%) and (20,30] years (20.861%) in order. Simultaneously, those images were randomly [split into three](#) sets, which of 80% for training, 20% for validation, respectively. The training set and validation set have no repetition and are consistent with each model that we trained.

Age	(0,10]	(10,20]	(20,30]	(30,40]	(40,50]
Male	13.451%	4.323%	11.451%	12.612%	8.308%
Female	8.736%	2.391%	9.410%	8.557%	6.055%
Age	(50,60]	(60,70]	(70,80]	(80,90]	>90
Male	4.322%	2.124%	0.634%	0.194%	0.009%
Female	4.421%	2.266%	0.583%	0.137%	0.015%
Total	Male: 57.43%;		Female: 42.57%		

Table 1 Sample characteristics.

This study confirmed that all methods were implemented in accordance with the relevant guidelines and regulations of the ethics committee of Shenzhen Bao'an District People's hospital. It is confirmed that all

the experimental protocols have been approved by the ethics committee of Shenzhen Bao'an District People's hospital. The informed consent was obtained from all subjects, and the informed consent of parents and / or legal guardian was obtained for those under 18 years old.

Labelling of images

Image samples of eardrums and EAC were divided into eight categories based on Colour Atlas of Endo-Otoscopy [13], as shown in **Figure 1**. All the images classification were implemented by six ear specialists with more than six years of experience

(1) Normal eardrum and EAC (included completely normal eardrum, normal with healed perforation or some tympanosclerosis, NE, **Figure 2**).

(2) Chronic suppurative otitis media (CSOM): There is perforation of tension of tympanic membrane and they are not uniform size. Most of them are single shot. The residual tympanic membrane may have calcification, ulceration and granulation tissue growth around the perforation margin.

(3) Cholesteatoma of middle ear (CME): Loose inner pocket can be seen, and white exfoliated epithelium can be seen inside the pocket.

(4) External auditory cana bleeding (EACB): Bright red blood can be clearly seen in the external auditory canal.

(5) Impacted cerumen (IC): The external auditory canal can be blocked by brown black or yellowish brown lumps. The cerumen masses have different textures, some are loose like mud; some are hard like stone.

(6) Otomycosis external (OE): The external auditory canal and tympanic membrane are covered with yellow black or white powdery or villous fungal masses. The short process of malleus is apparently exoid.

(7) Secretory otitis media (SOM): The tympanic membrane is invaginated and the handle of malleus moves backward and upward. When the tympanic cavity has effusion, the tympanic membrane loses its normal luster, showing light yellow, orange oil or amber color, but If the liquid does not fill in the tympanic cavity, the liquid level can be seen through the tympanic membrane.

(8) Tympanic membrane calcification (TMC): The calcification of tympanic membrane is deposited like white plaque, which is located in fibrous layer of tympanic membrane, but the reason is unclear. It may be related to chronic inflammation, such as chronic otitis media and so on, which can be found in entire intact and perforated tympanic membrane.

Training transfer learning network models

In order to [extract features](#) from eardrums and EAC white light images for the automated detection of ear diseases, we used a model method which is typically used to solve image classification in computer vision [14,15]. In many models of deep learning models, ResNet [16] (ResNet50, ResNet101), DensNet-BC

[17, 18] (DensNet-BC121, DensNet-BC161, DensNet-BC169), Inception-V3 [19], V4 [20], Inception-ResNet-V2 [20] and MoblieNet -V2 [21], V3 [22] were implemented and compared performance data from release to release, such as Inputting the image samples, training network, optimizing the network model. In this process, we used global average pooling in place of the fully connected layers in each model, generating output eight output nodes with a softmax activation function. The training makes full use of a stochastic gradient descent method [23] with a batch size of 100, epoch of 15, an initial learning rate of 0.01, momentum of 0.9 and weight decay of 10^{-4} to optimize parameters. This study was performed by means of the deep learning framework PyTorch [24] through four graphics processing unit (Tesla K80, NVIDIA) in Dell T640 station (inc., USA). For data augment in the process of model training, we performed random X and Y flip horizontal and vertical of input images.

Firstly, we classified the features of image samples of eardrums and EAC from the training sets by feeding to the deep neural network in the frame of PyTorch, and then we observed the performance of the training model on the validation dataset, simultaneously. And when the loss and the accuracy were stable, the training was stopped.

(1) Model structure adjustment

To reduce the size of image features slowly in the convolution operation process of training, we added one dense block ($[1 \times 1 \text{ conv}, 3 \times 3 \text{ conv}] \times 6$) which is the same as the first dense block of DenseNet-BC in DenseNet-BC [17, 18] framework. Take DensNetBC161 for example, added one dense block ($[1 \times 1 \text{ conv}, 3 \times 3 \text{ conv}] \times 6$) as the first dense block in DensNet-BC161, and the output size is 112×112 (tagged as DensNet-BC1615), as shown in **Figure 3**. Others, such as, DensNet-BC121 \rightarrow DensNet-BC1215, DensNet-BC169 \rightarrow DensNet-BC1915. Therefore, a total of 12 models were implemented and compared performance data from release to release adding the model described above.

(2) Selection of two appropriate models

Through the evaluation of the accuracy and calculation time performance among the 12 models, the appropriate models were selected. 80% and 20% of the images were set up the training set and validation set, respectively, from a total of 20,542 otoendoscopic images. Model optimization step was training-validation which was executed twice with training and validation set respectively.

(3) Ensemble classifier

An ensemble classifier was constructed by combining classifiers' outputs of the two appropriate models. Each classifier model assigns the probability of an input image to eight tags (NE, CME, CSOM, EACB, IC, OE, SOM, TMC) and the maximal probability among all tags is considered as a predictable label. The ensemble classifier combines 8-term score vectors from the predicted results of the two models together and the class with a maximal score will be treated as final forecast image's label.

(4) Sensitivity-specificity curve

Sensitivity and specificity are frequent clinimetric parameters that together define the ability of a measure to detect the presence or absence of a specific condition (i.e., likelihood ratio). On the whole testing set, a population-level sensitivity and specificity was calculated based on the following formula.

$$\text{Sensitivity} = \frac{TP}{TP + FN}, \quad \text{Specificity} = \frac{TN}{TN + FP}.$$

Where FP , FN , TP and TN represent the numbers of false positives, false negatives true positives and true negatives, respectively. A sensitivity-specificity curve can be created by changing the threshold value t (probability $p \geq t$, where t is a threshold value).

(5) Confusion matrix

We used confusion matrix to evaluate the quality of the output of the classifier. The values in the diagonal line represent the number of correctly predicted samples, while the values not in the diagonal elements represent the number of misclassified samples. If the diagonal values are very high, it indicates the classifier has a very good performance.

(6) Overall accuracy

The overall accuracy is the ratio of the number of correctly categorized images to the total number of testing images, as shown below:

$$\text{Overall Accuracy} = \frac{N_{\text{correctly classified images}}}{N_{\text{testing images}}}.$$

Results

Model and performance analysis

The number of parameters, training and validation time (Model optimization time) and accuracy of every transferred model were revealed in **Table 2**. The number of parameters was calculated by user-defined python programs, as shown below.

```
def get_model_parameter_num(net):
    total_num = sum(p.numel() for p in net.parameters())
    trainable_num = sum(p.numel() for p in net.parameters() if p.requires_grad)
    return {'Total Time': total_num, 'Train Time': trainable_num}
```

The hidden layer of the models had no significant improvement. There is not a hidden layer in the fully connected layer of the ten models. Calculating results show that the best accuracy was the DensNet-BC1615 (95.099%), followed by Inception-ResNet-V2 (94.617%), DensNet-BC161(94.564%) and DensNet-BC169 (94.541%), as shown in Table 2. For model optimization time, DensNet-BC1615, Inception-ResNet-V2, DensNet-BC161 and DensNet-BC169 were 80,895, 111,849 and 78,453 and 56,477 seconds, respectively. Together with the accuracy and the model optimization time, DensNet-BC1615 and DensNet-BC169 were selected to be the best transferred network models to form ensemble classifier.

Transferred models	Accuracy	GPU time (seconds)	Parameters
MoblieNet -V2	93.455	27,240	2,235,200
MoblieNet -V3	93.884	24,758	2,946,622
Inception-V4	93.000	98,270	42,681,353
ResNet50	93.581	51,098	25,557,032
ResNet101	93.632	78,844	42,516,552
Inception-ResNet-V2	94.617	111,849	54,318,760
DensNet-BC121	94.188	54,192	6,962,056
DensNet-BC161	94.564	78,453	26,489,672
DensNet-BC169	94.541	56,477	12,497,800
DensenetBC1215	94.364	56,079	7,548,920
DensenetBC1615	95.099	80,895	27,893,456
DensenetBC1695	94.339	58,209	13,122,040

Table 2 Performance table of training models. GPU time is the processing power needed for training and validation the model.

From the two models, classification mechanism of the ensemble classifier is estimated according to the following formula.

$$S = \max\{x | x \in S_1 * S_2\} \quad (1)$$

Where S_1 and S_2 are lexicographic vector of an input image predictor score of the two models, respectively. $S_1 * S_2$ represents the dot product of the S_1 and S_2 vectors. S is a predicted label score of the ensemble classifier. For this design, we also give an example of the ensemble classifier running results which was showed in **Figure 4**.

In this research, we calculate the confusion matrices for DensNet-BC1615, DensNet-BC169 and the ensemble classifier that are shown in **Figure 5**. The average classification accuracy was obtained on DensNet-BC1615, DensNet-BC169 and the ensemble classifier reached to 94.94%, 95.08%, and 95.59%, respectively. The combined forecasting method possessed the two single method's advantages, and the result showed that forecast value was more accurate.

We assessed the ensemble classifier according to the performance of generating binary predictions on Urgent versus Non-urgent subjects. Blood transfusion as the means of life-saving treatment of many diseases. Such a binary classification task has been very important for clinical significance, since emergency case should be treated immediately. Any delay, attributed to misclassification for example, will increase the risk of death. The performance of the Urgent versus Non-urgent based on the sensitivity-specificity curve can be clearly found in **Figure 6**. The AUCs of the DensNet-BC1615, DensNet-BC169 and the ensemble classifier were 0.9968, 0.9965, and 0.9974, respectively.

Real-time automatic identification system

A real-time automatic identification system was designed by combining endoscopy system and ensemble classifier, as shown in Figure 7, and its web page also can be seen in. The image was obtained from the endoscopy system by adjusting the focus. The image got into the real-time recognition system after being processed by capture system, and then the prediction results were obtained by the ensemble classifier, which was displayed on the web page of the system. Provided that an image is in the process of real-time classification, if the maximum probability of the eight classes (NE, CME, CSOM, EACB, IC, OE, SOM, TMC) estimated by one of the three models (DenseNet-BC169, DenseNet-BC1615 and ensemble classifier) is less than or equal to 0.3, or more than three categories of the prediction probabilities are greater than 0.3 in any model of the three, the system would point out that the image is likely to be excluded in those eight categories, and give tips on the web page of the system (others, as shown in the inset of **Figure 7**), which will arouse doctors' attention and give artificial intervention to avoid misjudgment.

In addition, in order to test the working stability of the real-time automatic identification system, we do a general analysis of the confusion matrices and the sensitivity-specificity curve using the clinical endoscopic images of the department of otolaryngology in the people's hospital of Shenzhen Baoan district in the past six months, as shown in **Figure 8**. The average classification accuracy and the AUCs were 95.127% and 0.9949, respectively. The actual test shows that the system achieves the desired objective and is stable and reliable. The response forecast time of the system is about 0.7 seconds for one endoscopic image.

Discussion

Diagnosis of ear disease mainly depends on otoscopy and physician's experience [25], especially external auditory canal. For the accuracy of the ear disease diagnosis, otolaryngologists executed demonstrably better than pediatricians and general practitioners, because diagnosis by otoendoscopy needed expertise in otology doctors [26]. In this condition, deep network model could provide physicians with suggesting potential diagnosis according to otoendoscopic image.

In the current model, a dataset of 20,542 labelled otoendoscopic images from more than 40,000 patients were used. Otoendoscopic images of the eardrum and external auditory canal were classified into six categories. The classification accuracy of the current model has reached 95.59%. Previous studies make

use of 10,544, 389 and 391 images to analyze ear diseases, with the accuracy of 93.73%, 86.84% and 80.6% [27-29], respectively. Unluckily, this is only for scientific research and has not been translated into applications. In our work, we also build a real-time interactive detection system that provides doctors with real-time diagnostic results for complementary medical benefits. The classification accuracy of our model reached to 95.59%.

There are a few notable limitations to this study. These include collection of the video frame by a simple operator who is also an acknowledged expert in otology and the use of video frame recordings instead of real-time assessments of ear disease. Nevertheless, we hope that the competence to operate and stabilize the instrument to let stable imaging of the eardrum and external auditory canal in focus will be obtainable by an otoscope inspector with a generally-used skill. Even though this is not the real time detecting of the eardrum and external auditory canal in clinical treatment because this model has not yet been utilized in an actual patient deployment scenario, as is mentioned above, the testing dataset is untouched, raw and our model executes in almost real-time.

Looking ahead, an approach similar to deep learning also has great potential in improving endoscopic otologic diagnosis. In addition, alternative endoscopic images, confocal laser and endocytoscopy, for example, are most likely to be utilized to train this platform to supply explanation of clinically acquired images.

In summary, this study shows that a real-time deep learning system of ear disease diagnosis according to otoscopy can realize high accuracy in sorting the disease of the eardrum and external auditory canal when used on unaltered otoscopy. video sequences. In view of its high accuracy, we plan to conduct clinical trials to assess the potential of this imaging analytics artificial intelligence model in day-to-day practice.

Declarations

Author contributions

X.Z., H.G. Li, F.W. and Z.L. designed the study, collected the data, analyzed the data and wrote the manuscript. J.S., K.W., T.L. and X.L. collected the data. W.L. and Z.J. designed deep transfer learning system and performed training with Z.L. H.Y. Li, G.L and Z.J. designed and developed real-time automatic identification system. All authors read and approved the final version of the manuscript.

Funding

This work is supported by the foundation for young creative talents of department education of guangdong (Natural Science), China, Grant No. 2019KQNCX067.

Competing interests

The authors declare no competing interests.

Correspondence and requests for materials should be addressed to Z.L.

Reprints and permissions information is available at www.nature.com/reprints.

Publisher's note Springer Nature remains neutral with regard to jurisdictional claims in published maps and institutional affiliations.

References

1. Samy S, Abu Naser, Hasan A, Abu Hasanein. Ear Diseases Diagnosis Expert System Using SL5 Object. *World Wide Journal of Multidisciplinary Research and Development* **2**, 41-47 (2016).
2. Blomgren K, Pitkäranta A. Is it possible to diagnose acute otitis media accurately in primary health care? *Fam Pract* **20**, 524-7 (2003).
3. Pichichero ME, Poole MD. Assessing diagnostic accuracy and tympanocentesis skills in the management of otitis media. *Arch Pediatr Adolesc Med* **155**, 1137-1142 (2001).
4. LeCun Y, Bengio Y, Hinton G. Deep learning. *Nature* **521**, 436-44 (2015).
5. He K, Zhang X, Ren S, et al. Delving deep into rectifiers: surpassing human-level performance on ImageNet classification. In: *Proceedings of the IEEE International Conference on Computer Vision*; <https://www.cv-foundation.org/openaccess/> (2015).
6. Kooi T, Litjens G, van Ginneken B, et al. Large scale deep learning for computer aided detection of mammographic lesions. *Med Image Anal* **35**, 303-312 (2017).
7. Gulshan V, Peng L, Coram M, et al. Development and validation of a deep learning algorithm for detection of diabetic retinopathy in retinal fundus photographs. *JAMA Internal Medicine* **316**, 2402-2410 (2016).
8. LeCun Y, Bengio Y, Hinton G. Deep learning. *Nature* **521**, 436-444 (2015).
9. Gong Y, Wang L, Guo R, et al. Multi-scale orderless pooling of deep convolutional activation features. In: Fleet D, Pajdla T, Schiele B, Tuytelaars T, eds. *Computer Vision-ECCV*. New York: Springer (2014).
10. Sharif Razavian A, Azizpour H, Sullivan J, et al. CNN features off-the-shelf: an astounding baseline for recognition. In: *Proceedings of the IEEE Conference on Computer Vision and Pattern Recognition Workshops*. <https://www.cv-foundation.org/openaccess/> (2014).
11. Cimpoi M, Maji S, Vedaldi A. Deep filter banks for texture recognition and segmentation. In: *Proceedings of the IEEE Conference on Computer Vision and Pattern Recognition*. <https://openaccess.thecvf.com/> (2015).
12. Sermanet P, Eigen D, Zhang X, et al. Overfeat: integrated recognition, localization and detection using convolutional networks. arXiv. Available at: <https://arxiv.org/abs/1312.6229> (2017).
13. Sanna M, Russo A, Caruso A, Taibah A, Piras G. Color atlas of endo-otoscopy. Examination-Diagnosis-Treatment, 8-11, 14-54, 66-74, 81-92, 94-112, 118-138, 160-166, 195-197, (2017).
14. Ren S, He K, Girshick R, et al. Faster R-CNN: towards real-time object detection with region proposal networks. *Neural information processing systems* **28**, 91-99 (2015).

15. Li J, Zhang J, Chang D, *et al.* Computer-Assisted Detection of Colonic Polyps Using Improved Faster R-CNN. *Chinese Journal of Electronics* **28**, 718-724 (2019).
16. He K, Zhang X, Ren S, Sun J. Deep residual learning for image recognition. *Proceedings of the IEEE conference on computer vision and pattern recognition*, <https://arxiv.org/> (2016).
17. Huang, Z. Liu, L. V. Der Maaten, K. Q Weinberger, Densely Connected Convolutional Networks, *Proceedings of the IEEE computer vision and pattern recognition*. <https://arxiv.org/abs/1608.06993> (2017).
18. Geoff Pleiss, Danlu Chen, Gao Huang, *et al.* Memory-efficient implementation of densenets. <https://arxiv.org/abs/1707.06990> (2017).
19. Szegedy C, Vanhoucke V, Ioffe S, Shlens J, Wojna Z. Rethinking the inception architecture for computer vision. *Proceedings of the IEEE conference on computer vision and pattern recognition*. <https://arxiv.org/abs/1512.00567> (2016).
20. Szegedy C, Ioffe S, Vanhoucke V, Alemi AA. Inception-v4, Inception-ResNet and the Impact of Residual Connections on Learning. *Thirty-first AAAI conference on artificial intelligence*. <https://arxiv.org/abs/1602.07261> (2017).
21. Sandler M, Howard A, Zhu M, *et al.* Chen L-C. Mobilenetv2: Inverted residuals and linear bottlenecks. *Proceedings of the IEEE conference on computer vision and pattern recognition*. <https://arxiv.org/abs/1801.04381> (2018).
22. Howard, M. Sandler, G. Chu, *et al.* Searching for MobileNetV3. International conference on computer vision. <https://ieeexplore.ieee.org/document/9008835> (2019).
23. Bottou L. Large-Scale Machine Learning with Stochastic Gradient Descent. In: Lechevallier Y., Saporta G. (eds) *Proceedings of COMPSTAT'2010*. Physica-Verlag HD. https://doi.org/10.1007/978-3-7908-2604-3_16 (2010).
24. Ketkar N. Introduction to PyTorch. In: *Deep Learning with Python*. Apress, Berkeley, CA. https://doi.org/10.1007/978-1-4842-2766-4_12 (2017).
25. Marom T, Kraus O, Habashi N, Tamir SO. Emerging technologies for the diagnosis of otitis media. *Otolaryngol Head Neck Surg* **160**, 447-456 (2019).
26. Pichichero ME, Poole MD. Comparison of performance by otolaryngologists, pediatricians, and general practitioners on an otoendoscopic diagnostic video examination. *Int J Pediatr Otorhinolaryngol* **69**, 361-366 (2005).
27. Myburgh HC, van Zijl WH, Swanepoel D, Hellstrom S, Laurent C. Otitis media diagnosis for developing countries using tympanic membrane image-analysis. *EBioMedicine* **5**, 156-160 (2016).
28. Myburgh HC, Jose S, Swanepoel DW, Laurent C. Towards low cost automated smartphone- and cloud-based otitis media diagnosis. *Biomed Sig Process Control* **39**, 34-52 (2018).
29. Cha, C. Pae, S. Seong, J. Young Choi, Ha. Park. Automated diagnosis of ear disease using ensemble deep learning with a big otoendoscopy image database *EBioMedicine* **45**, 606-614 (2019).

Figures

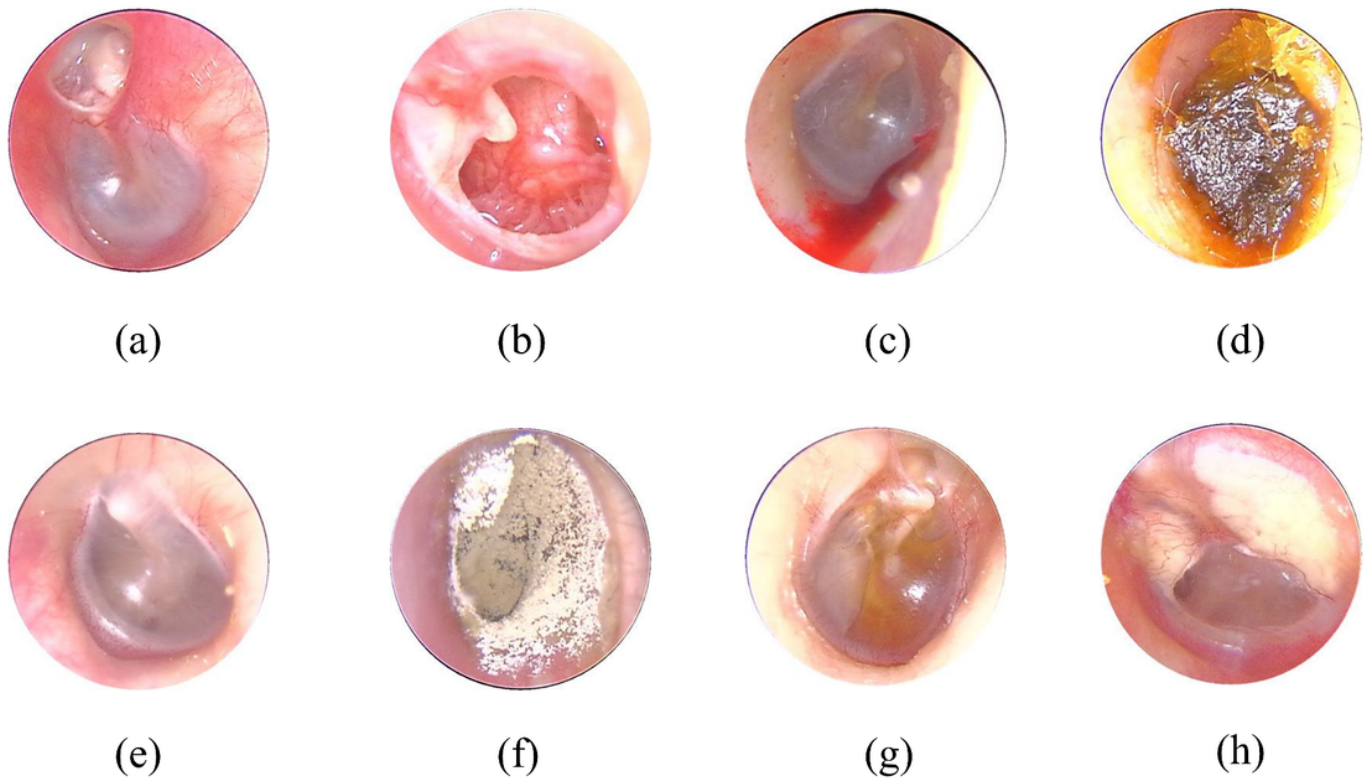


Figure 1

Otoendoscopy image and eight diagnostic classes of ear diseases. (a) Cholesteatoma of ear (n=818). (b) Chronic suppurative otitis media (n=3169). (c) External auditory cana bleeding (n=694). (d) Impacted cerumen (n=5453). (e) Normal eardrum (n=4217). (f) Otomycosis external (n=2256). (g) Secretory otitis media (n=2448). (h) Tympanic membrane calcification (n=1037).

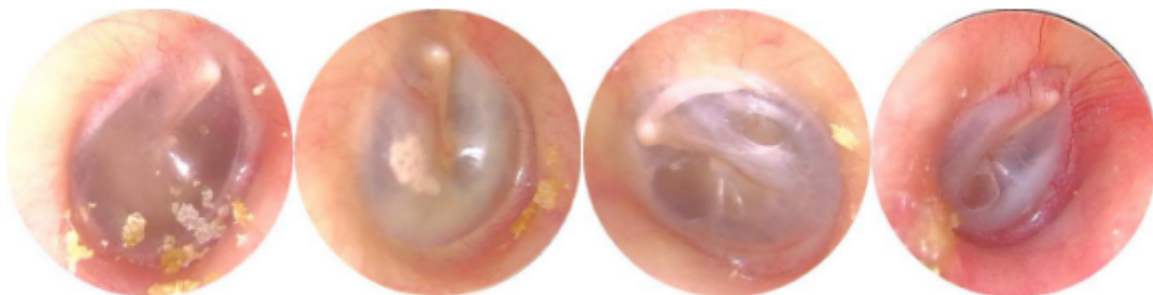


Figure 2

Example of image diversity labelled "Normal".

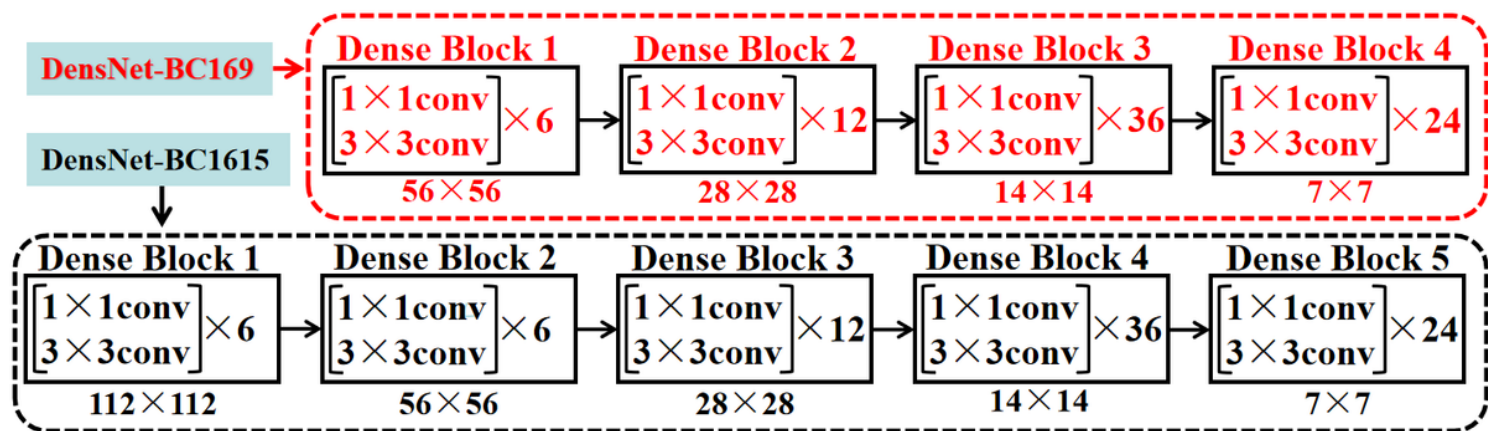


Figure 3

A schematic of model structure adjustment for DensNet-BC1615.

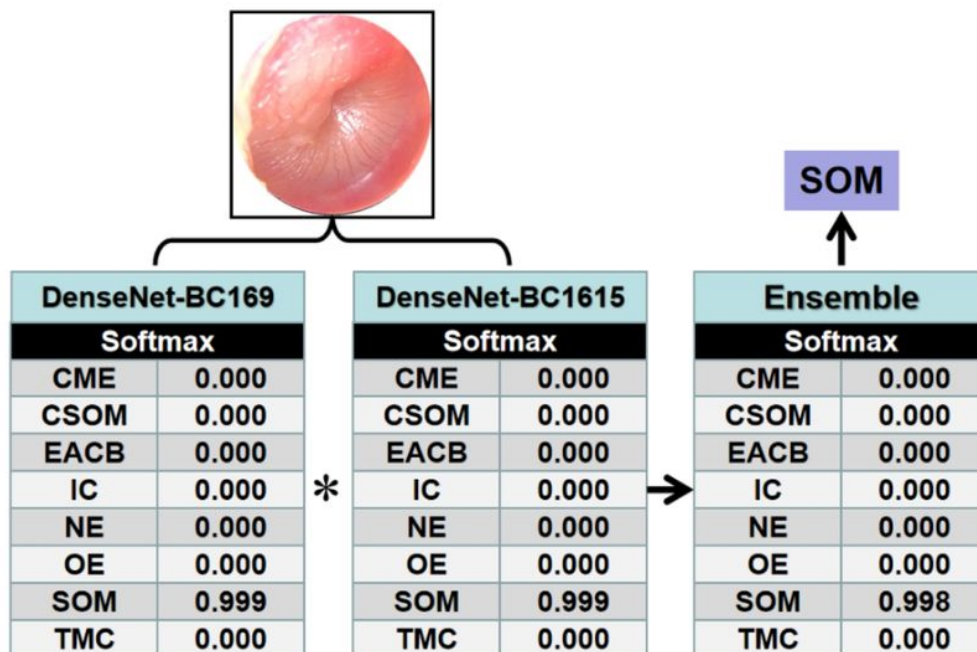


Figure 4

A sketch of structure and an operating diagram for the ensemble method classifies given otoendoscopic image.

	DnesNet-BC169									DnesNet-BC1615									Ensemble Classifier								
CME	157 3.82%	3 0.07%			4 0.10%	2 0.05%	1 0.02%	4 0.10%	171 91.81% 8.19%	164 3.99%	5 0.12%			2 0.05%	4 0.10%	1 0.02%		176 93.18% 6.82%	162 3.94%	4 0.10%			4 0.10%	2 0.05%	1 0.02%		173 93.64% 6.36%
CSOM	2 0.05%	708 17.23%		1 0.02%		2 0.05%	3 0.07%	11 0.27%	727 97.39% 2.61%		703 17.11%			1 0.02%	1 0.02%	3 0.07%	5 0.12%	713 98.60% 1.40%		707 17.21%		1 0.02%		1 0.02%	1 0.02%	6 0.15%	716 98.74% 1.26%
EACB		1 0.02%	138 3.36%						139 99.28% 0.72%		3 0.07%	138 3.36%			1 0.02%	2 0.05%		144 95.83% 4.17%		1 0.02%	138 3.36%				2 0.05%		141 97.87% 2.13%
IC		2 0.05%		1057 25.73%		25 0.61%		1 0.02%	1085 97.42% 2.58%		3 0.07%		1063 25.88%		34 0.83%	1 0.02%		1101 96.55% 3.45%		2 0.05%		1065 25.93%		29 0.71%			1096 97.17% 2.83%
NE		3 0.07%		1 0.02%	794 19.33%	1 0.02%	34 0.83%	5 0.12%	838 94.75% 5.25%		1 0.02%		1 0.02%	801 19.50%	1 0.02%	42 1.02%	5 0.12%	851 94.12% 5.88%		2 0.05%		1 0.02%	803 19.55%	1 0.02%	37 0.90%	5 0.12%	849 94.58% 5.42%
OE		1 0.02%		29 0.71%		418 10.18%	3 0.07%	1 0.02%	452 92.48% 7.52%		3 0.07%		26 0.63%		408 9.93%	2 0.05%	1 0.02%	440 92.73% 7.27%		3 0.07%		23 0.56%		415 10.10%	1 0.02%	1 0.02%	443 93.68% 6.32%
SOM	3 0.07%	2 0.05%		2 0.05%	41 1.00%		446 10.86%	3 0.07%	497 89.74% 10.26%		4 0.10%		1 0.02%	28 0.68%		436 10.61%	3 0.07%	472 92.37% 7.63%		2 0.05%	2 0.05%		31 0.75%		445 10.83%	3 0.07%	484 91.94% 8.06%
TMC	2 0.05%	4 0.10%		1 0.02%	4 0.10%	3 0.07%	3 0.07%	182 4.43%	199 91.46% 8.54%		2 0.05%			11 0.27%	2 0.05%	3 0.07%	193 4.70%	211 91.47% 8.53%		3 0.07%			5 0.12%	3 0.07%	3 0.07%	192 4.67%	206 93.20% 6.80%
	164 95.73% 4.27%	724 97.79% 2.21%	138 100% 0.00%	1091 96.88% 3.12%	843 94.19% 5.81%	451 92.68% 7.32%	490 91.02% 8.98%	207 87.92% 12.08%	4108 94.94% 5.06%	164 100% 0.00%	724 97.10% 2.90%	138 100% 0.00%	1091 97.43% 2.57%	843 95.02% 4.98%	451 90.47% 9.53%	490 88.98% 11.02%	207 93.24% 6.76%	4108 95.08% 4.92%	164 98.78% 1.22%	724 97.65% 2.35%	138 100% 0.00%	1091 97.62% 2.38%	843 95.26% 4.74%	451 92.02% 7.98%	490 90.82% 9.18%	207 92.75% 7.25%	4108 95.59% 4.41%
	CME	CSOM	EACB	IC	NE	OE	SOM	TMC		CME	CSOM	EACB	IC	NE	OE	SOM	TMC		CME	CSOM	EACB	IC	NE	OE	SOM	TMC	

Figure 5

Confusion matrices for DensNet-BC169, DensNet-BC1615, and ensemble classifier at the test sample sets having a maximal accuracy.

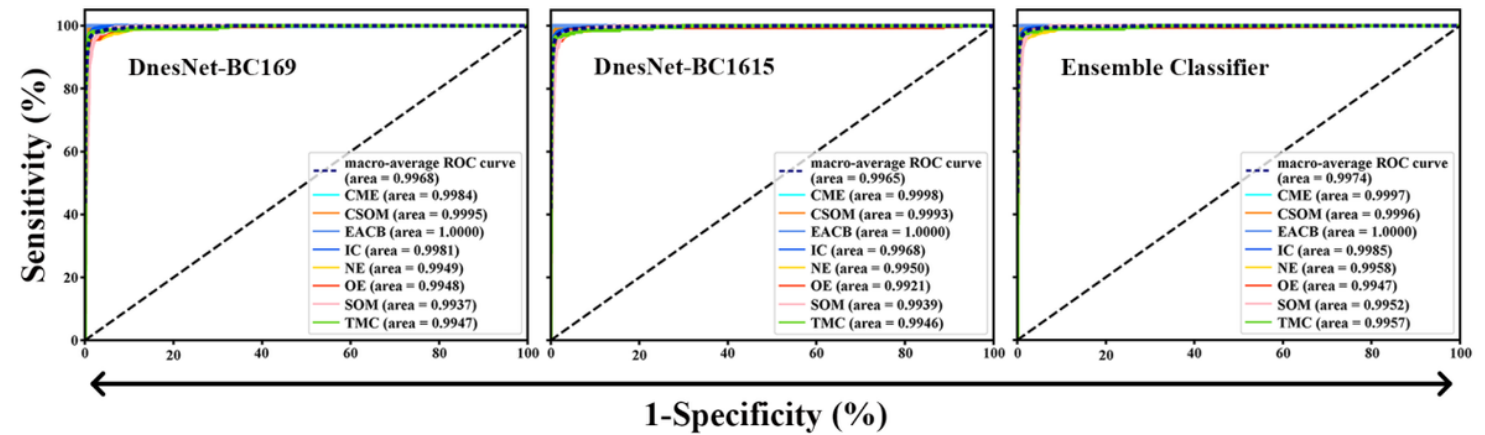


Figure 6

The sensitivity-specificity curve of the ensemble classifier at the test sample sets for Urgent versus Non-urgent binary classification.

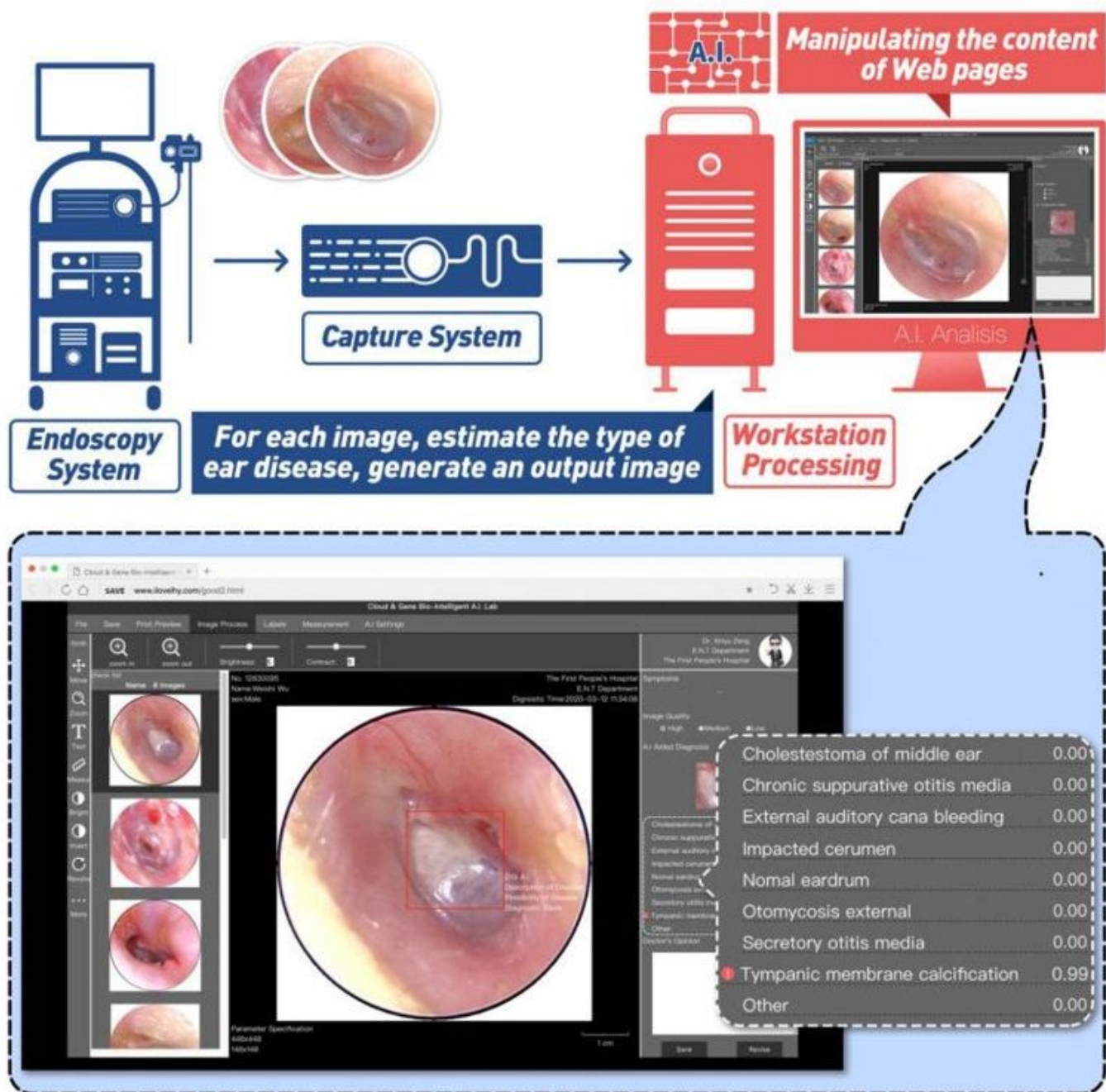


Figure 7

A schematic diagram of the real-time automatic identification system for ear diseases and the system web page of the system. The red border is drawn manually by the doctor.

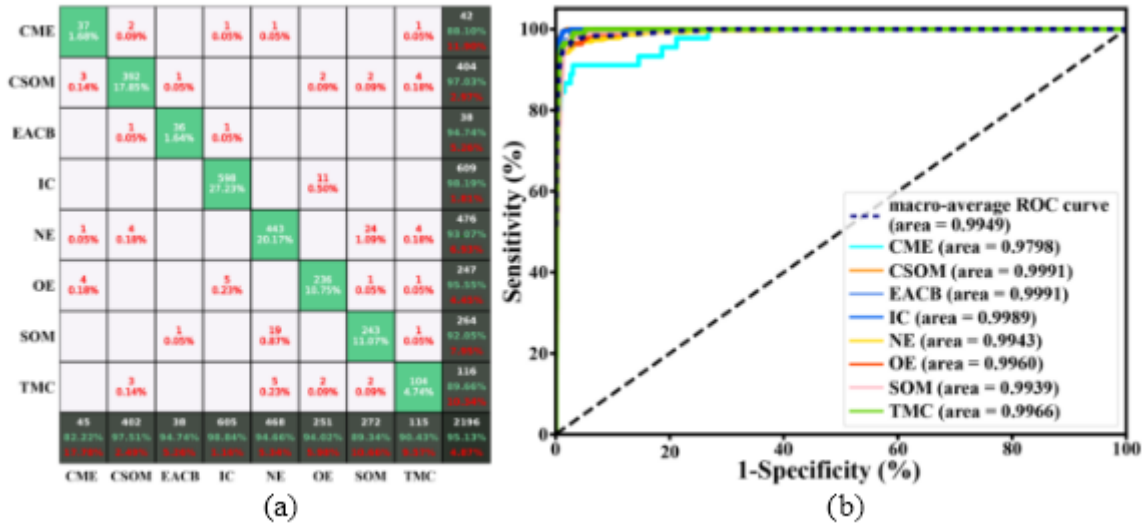


Figure 8

The Confusion matrices (a) and sensitivity-specificity (b) curve of the real-time automatic identification system based on the ensemble classifier at endoscopic images about the past six months.